Dalton Transactions

ROYAL SOCIETY OF CHEMISTRY

PAPER

View Article Online
View Journal | View Issue

Check for updates

Cite this: *Dalton Trans.*, 2022, **51**, 10186

Balancing the interplay between ligand ejection and therapeutic window light absorption in ruthenium polypyridyl complexes†

Annie B. McCullough,‡[a] Jiaqi Chen, ‡[b] Nathaniel P. Valentine,[a] Toney M. Franklin,[a] Andrew P. Cantrell,[a] Vayda M. Darnell, [a] Qasim Qureshi,[c] Kenneth Hanson, [b] Steven M. Shell[c] and Dennis L. Ashford *[a]

Received 20th April 2022, Accepted 14th June 2022

DOI: 10.1039/d2dt01237e

rsc.li/dalton

Ruthenium polypyridyl complexes have gained significant interest as photochemotherapies (PCTs) where their excited-state properties play a critical role in the photo-cytotoxicity mechanism and efficacy. Herein we report a systematic electrochemical, spectrochemical, and photophysical analysis of a series of ruthenium(II) polypyridyl complexes of the type $[Ru(bpy)_2(N{-}N)]^{2+}$ (where bpy = 2,2′-bipyridine; N–N is a bidentate polypyridyl ligand) designed to mimic PCTs. In this series, the N–N ligand was modified through increased conjugation and/or incorporation of electronegative heteroatoms to shift the metal-to-ligand charge-transfer (MLCT) absorptions near the therapeutic window for PCTs (600–1100 nm) while incorporating steric bulk to trigger photoinduced ligand dissociation. The lowest energy MLCT absorptions were red-shifted from λ_{max} = 454 nm to 564 nm, with emission energies decreasing from λ_{max} = 620 nm to 850 nm. Photoinduced ligand ejection and temperature-dependent emission studies revealed an important interplay between red-shifting MLCT absorptions and accessing the dissociative ^{3}dd* states, with energy barriers between the ^{3}MLCT* and ^{3}dd* states ranging from 850 cm^{-1} to 2580 cm^{-1} for the complexes measured. This work demonstrates the importance of understanding both the MLCT manifold and ^{3}dd* state energy levels in the future design of ligands and complexes for PCT.

Introduction

Transition metal coordination complexes have emerged as a promising class of chemotherapeutics for the treatment of cancer and other diseases.[1,2] Nearly half of all chemotherapeutics administered today are derived from the platinum-based drug family (platins), which still suffer from major drawbacks, most notably harsh side effects due to a lack of specificity for malignant cells over healthy ones.[3–10] Photochemotherapy (PCT) and photodynamic therapy (PDT) have the potential to circumvent these issues by utilizing a compound that is minimally toxic in the dark and in its native state, but becomes cytotoxic upon illumination, providing spatiotemporal control of toxicity.[11–14] Traditionally, PDTs rely on the photoinduced excited-state electron transfer (Type I) or excited-state triplet energy transfer (Type II) to molecular oxygen ($^3O_2$) to generate reactive oxygen species (ROS) and trigger oxidative cell death.[11] While PDTs have been used in clinical oncology for over 40 years, they have largely remained absent from main-stream cancer treatments due to two major factors; (1) the inherent hypoxic nature of tumor cells and (2) a lack of photosensitizers (PSs) that absorb light in the near-IR, therapeutic window (600–1100 nm).[15–22] In contrast, PCTs mechanism of toxicity involves the photoinduced release of a therapeutic reagent, making it oxygen-independent and circumventing the issue of low cellular oxygen concentrations.[21,23–29] Ru(II) polypyridyl compounds have shown great promise as PCTs due to their synthetic viability, relatively long-lived triplet metal-to-ligand charge transfer (^{3}MLCT*) excited states, and well understood photophysical behavior.[30–36]

Ru(II) PCTs typically undergo photoinduced ligand loss to either release a known cytotoxic organic compound from the coordination sphere[24,37–41] or generate a di-solvated activated metal species that can have cisplatin-like interactions with DNA at the newly opened coordination sites (Fig. 1).[23,29,42–44] While this mechanism has been shown to have high phototoxi-

---

[a] *Department of Natural Sciences, Tusculum University, Greeneville, Tennessee37745, USA. E-mail: dashford@tusculum.edu*

[b] *Department of Chemistry & Biochemistry, Florida State University, Tallahassee, Florida 32306, USA*

[c] *Department of Natural Sciences, University of Virginia's College at Wise, Wise, Virginia, 24293, USA*

† Electronic supplementary information (ESI) available. See DOI: **https://doi.org/10.1039/d2dt01237e**

‡ Authors contributed equally.

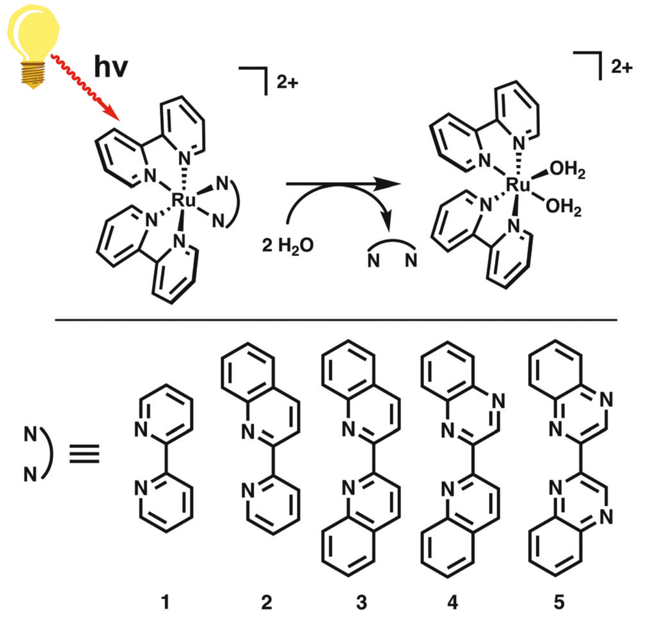

Fig. 1 Photoinduced ligand ejection from Ru(II) center and structures of $[Ru(bpy)_2(N–N)]^{2+}$ complexes **1–5**.

city indexes, most reported Ru(II) PCTs only absorb in the blue region of the electromagnetic spectrum (<485 nm), which penetrates skin much shallower than longer wavelengths.[22] Near-IR ligand ejection has been reported for Ru(II) PCTs, however, these complexes still have relatively low oscillator strengths at wavelengths >500 nm and center around the ejection of a monodentate ligand as opposed to bidentate ligand ejection required for metalation of DNA.[21,25,37,42,45,46]

Photoinduced ligand ejection from the octahedral Ru(II) center requires thermal population of the formally antibonding ^{3}dd* states from the ^{3}MLCT* excited states.[30,47–49] This is typically achieved by increasing steric bulk around the Ru(II) center, distorting the pseudo-octahedral, and ultimately lowering the energy of the ^{3}dd* states. In addition, incorporation of increased conjugation and/or electronegative heteroatoms within the ligand framework lowers the energies of the ligand π* orbitals, increasing their π*-acceptor ability, and resulting in lower MLCT energy absorption features.[30,50–52] Furthermore, the compound must be soluble in biological (aqueous) medium and a balance between thermal stability of the native complex and photoactivation kinetics must be maintained. Papish and co-workers recently published density functional theory (DFT) analyses of a series of Ru(II) polypyridyl complexes bearing acidic protons and note the importance of understanding these excited-state energy levels in PCT design and the pronounced effect they can have on the mechanism of photo-toxicity.[53]

With this in mind, we set out to design a series of compounds with the general structure $[Ru(bpy)_2(N–N)]^{2+}$ (where N–N is a bidentate polypyridyl ligand, Fig. 1) that systematically increases steric bulk around the Ru(II) center while also introducing increased conjugation and/or electronegative heteroatoms. The goal being to understand their electrochemical, spectrochemical, ligand ejection kinetics, photophysical properties, and ability to act as PCTs. This work demonstrates that traditional ligand design strategies to red-shift MLCT absorptions by lowering the energy of the ligand π* orbitals can also impact ligand dissociation kinetics by limiting the accessibility of the ^{3}dd* states, and ultimately the ability of a complex to act as a PCT agent. The present study further highlights the importance of understanding this relationship between ligand ejection kinetics and lower energy absorption in Ru(II) PCTs, which will aid in the design strategies of future PCT ligands and complexes.

Results and discussion

Ligand synthesis

2,2′-Bipyridine (**L1**) and 2,2′-biquinoline (**L3**) were purchased and used without further purification. 2-(Quinolin-2-yl)quinoxaline (**L4**) was synthesized by a reported procedure in 85% yield.[30] 2-(Pyridine-2-yl)quinoline (**L2**) was synthesized in 96% yield using a Friedländer condensation of 2-acetylpyridine and 2-aminobenzaldehyde in the presence of a base catalyst (Scheme 1). 2,2′-Biquinoxaline (**L5**) was prepared in 10% yield using minor modifications of literature procedure[54] (*i.e.*, homocoupling of the hydrochloride salt of quinoxaline), with the experimental details provided in the ESI.†

Complex synthesis

The $[Ru(bpy)_2(N–N)]^{2+}$ complexes were prepared as their chloride salts by the reaction of $Ru(bpy)_2Cl_2$[55] with 1 equivalent of the corresponding N–N ligand in 1 : 1 EtOH : H_2O in a microwave oven reactor at 140 °C for 1 hour (Scheme 2). The reaction progress was monitored using UV-vis spectroscopy for the disappearance of the $Ru(bpy)_2Cl_2$ absorption features (λ_{max} = 363 and 526 nm in CH_3CN)[56] and the appearance of the absorption peaks attributed to complexes **1–5**. The crude mixtures

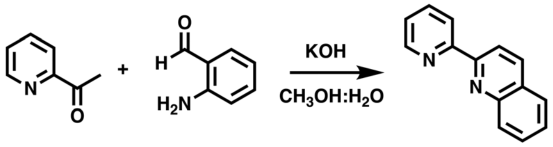

Scheme 1 Synthesis of **L2**.

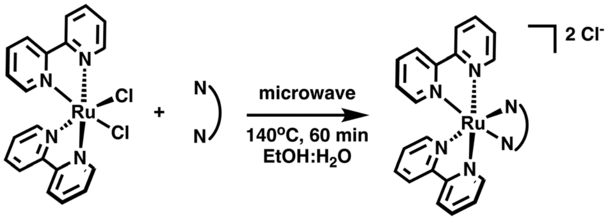

Scheme 2 General procedure for the synthesis of complexes **1–5**.

were then purified by size exclusion chromatography (Sorbadex S-25 fine) to yield pure complexes. It should be noted that all of the complexes are readily soluble in aqueous media, which is important for biological applications.

Electrochemistry

The electrochemical properties of complexes **1–5** were analyzed in dry CH_3CN (0.1 M $TBAPF_6$ supporting electrolyte, where $TBAPF_6$ = tetrabutyl ammonium hexafluorophosphate) by cyclic and square-wave voltammetry. The $E_{1/2}$ for the $Ru^{3+/2+}$ redox couple (eqn (1)) for each complex are reported in Table 1 with cyclic voltammograms shown in Fig. 2.

$$[Ru^{III}(bpy)_2(N\text{–}N)]^{3+} + e^- \rightarrow [Ru^{II}(bpy)_2(N\text{–}N)]^{2+} \tag{1}$$

All complexes exhibit reversible $Ru^{3+/2+}$ redox couples with $E_{1/2}$ values ranging from 1.29 V for **1** to 1.60 V for **5** (*vs.* SCE). Complexes **2–5** exhibit a more positive $Ru^{3+/2+}$ couple compared to the parent $[Ru(bpy)_3]^{2+}$ (**1**). This shift due to changes in N–N can be rationalized by the increased conjugation and/or the addition of electronegative heteroatoms compared to bpy, decreasing the energy of π* orbitals of N–N. This results in increased dπ–π* back bonding from the Ru^{II} center to the N–N ligand, stabilizing the $d\pi^6$ electronic configuration, and ultimately increasing the redox potential for the $Ru^{3+/2+}$ couple.[30,58–60]

Table 1 Electrochemical properties of **1–5** in N_2 deaerated CH_3CN (0.1 M $TBAPF_6$ electrolyte)

Compound	$E_{1/2}$ ($Ru^{3+/2+}$)	$E_{1/2}$ ($Ru^{2+/+}$)	$E_{1/2}$ ($Ru^{+/0}$)	$E_{1/2}$ ($Ru^{0/1-}$)
1	1.29	−1.35	−1.55	−1.78
2	1.32	−1.12	−1.50	−1.74
3	1.37	−0.92	−1.38	−1.69
4	1.48	−0.64	−1.24	−1.62
5	1.60	−0.46	−1.08	−1.61

In CH_3CN deaerated with N_2 for 10 min, 1 mM in complex and 0.1 M $TBAPF_6$ supporting electrolyte, glassy carbon working electrode, graphite rod counter electrode, and $Ag/AgNO_3$ (0.01 M $AgNO_3$ with 0.1 M $TBAPF_6$ in CH_3CN) reference electrode (values were adjusted to agree with literature values for $[Ru(bpy)_3]^{3+/2+}$ at 1.29 V *vs.* SCE).[34,51,56,57] $E_{1/2}$ values are from differential pulse voltammetry.

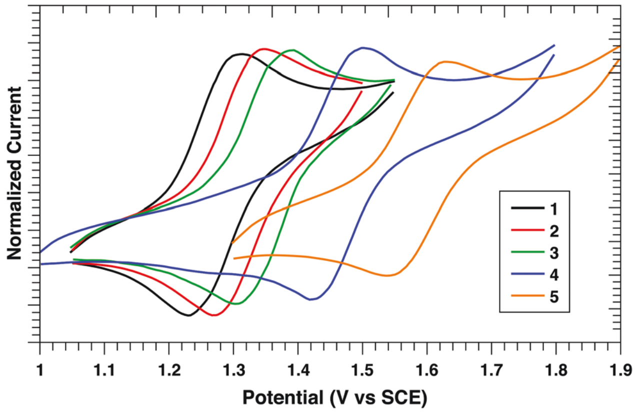

Fig. 2 Cyclic voltammograms acquired at 100 mV s^{-1} for 1 mM solutions of **1–5** in N_2 deaerated CH_3CN with 0.1 M $TBAPF_6$ supporting electrolyte. GC working electrode, graphite rod counter electrode, and $Ag/AgNO_3$ reference electrode (0.01 M $AgNO_3$ with 0.1 M $TBAPF_6$ in CH_3CN). Values were adjusted to agree with literature values for $[Ru(bpy)_3]^{3+/2+}$ at 1.29 V *vs.* SCE.[57]

Each complex exhibits three reversible ligand-based reductions with representative CVs shown in Fig. 3 (all shown in Fig. S1†) and potentials listed in Table 1. The first ligand-based reduction ($Ru^{2+/+}$, eqn (2)) for **2–5** are at more positive potentials compared to **1** (−1.35 V *vs.* SCE), ranging from −1.12 V for **2** to −0.46 V (*vs.* SCE) for **5**. The significantly more positive reduction potential for **4** (−0.64 V *vs.* SCE) and **5** (−0.46 V *vs.* SCE) are noteworthy given the possibility for these complexes to be reduced intracellularly by biological reducing agents such as NADH (≈−0.56 V *vs.* SCE in H_2O[61]) or GSH (≈−0.48 V *vs.* SCE in H_2O[62]). Again, the increased conjugation and incorporation of heteroatoms stabilizes the π* acceptor levels of N–N, resulting in lower reduction potentials of the N–N ligand.

$$[Ru^{II}(bpy)_2(N\text{–}N)]^{3+} + e^- \rightarrow [Ru^{II}(bpy)_2(N\text{–}N^{\bullet -})]^{+} \tag{2}$$

The variation in the first reduction potentials ($Ru^{2+/+}$, 0.89 V) is significantly larger than the variance for the second reduction ($Ru^{+/0}$, 0.47 V) and third reduction ($Ru^{0/1-}$, 0.17 V) potentials for the series (see Table 1 and Fig. S2†). This demonstrates, as expected, that the first reduction of the complex is largely N–N ligand-centered (eqn (2)), with the

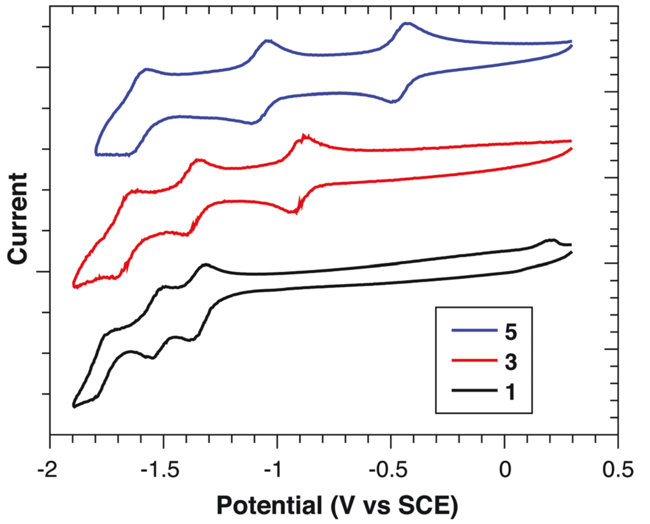

Fig. 3 Cyclic voltammograms acquired at 100 mV s^{-1} for 1 mM solutions of **1** (black), **3** (red), and **5** (blue) in N_2 deaerated CH_3CN with 0.1 M $TBAPF_6$ supporting electrolyte. GC working electrode, graphite rod counter electrode, and $Ag/AgNO_3$ reference electrode (0.01 M $AgNO_3$ with 0.1 M $TBAPF_6$ in CH_3CN). Values were adjusted to agree with literature values for $[Ru(bpy)_3]^{3+/2+}$ at 1.29 V *vs.* SCE.[57]

second and third reductions occurring mainly on the remaining bpy ligands (eqn (3) and (4)).

$$[\mathrm{Ru^{II}(bpy)_2(N{-}N^{\bullet-})}]^{+} + \mathrm{e^-} \rightarrow [\mathrm{Ru^{II}(bpy)(bpy^{\bullet-})(N{-}N^{\bullet-})}]^{0} \tag{3}$$

$$[\mathrm{Ru^{II}(bpy)(bpy^{\bullet-})(N{-}N^{\bullet-})}]^{0} + \mathrm{e^-} \rightarrow [\mathrm{Ru^{II}(bpy^{\bullet-})(bpy^{\bullet-})(N{-}N^{\bullet-})}]^{1-} \tag{4}$$

UV-Vis absorption

UV-Vis absorption spectra of complexes **1–5** in water (Fig. 4) all feature intense $\pi \rightarrow \pi^*$ absorption features below 350 nm ($\varepsilon \approx 4.0 \times 10^4$–$7.0 \times 10^4\ \mathrm{M^{-1}\ cm^{-1}}$). Complexes **3–5** exhibit additional, lower energy and structured absorption transitions at 350–450 nm that are attributed to the $\pi \rightarrow \pi^*$ transition of the N–N ligands.[30] The complexes also exhibit broad, lower-energy metal-to-ligand charge-transfer (MLCT) transitions ranging from 400 nm to 600 nm ($\varepsilon \approx 0.56 \times 10^4$–$11.6 \times 10^4\ \mathrm{M^{-1}\ cm^{-1}}$) and are formally assigned as $[\mathrm{d}\pi^6] \rightarrow [\mathrm{d}\pi^5\pi_1{}^*]^1$ transitions.[49,52,63] The appearance of the nominally spin forbidden $[\mathrm{d}\pi^6] \rightarrow [\mathrm{d}\pi^5\pi_1{}^*]^3$ transition at longer wavelengths (>600 nm) is due to spin–orbit coupling, but still have low oscillator strengths and therefore low molar absorptivities.[49,52,63] As mentioned previously, shifting the absorptions to lower energies is desirable to move excitation and photo-induced ligand ejection towards the therapeutic window of PCTs (>600 nm). This trend is observed in Fig. 4 by the red shift in the series from ^{1}MLCT $\lambda_{\max}$ = 454 nm (**1**) to $\lambda_{\max}$ = 564 nm (**5**).

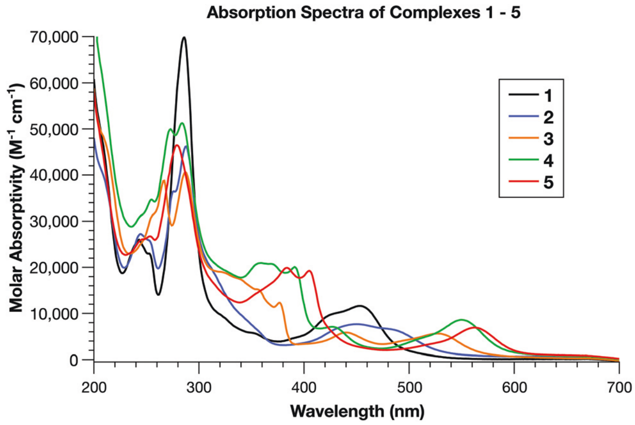

Fig. 4 UV-vis absorption spectra of complexes **1–5** in H_2O.

The energies of the MLCT transition are influenced by both an increase in conjugation within the N–N ligand, and the incorporation of non-coordinating electronegative heteroatoms. These perturbations lower the energies of the π^* orbitals on the N–N ligand, increasing the π^*-acceptor ability of the ligand, resulting in lower MLCT energy absorption features.[30,50–52] Complexes **3**, **4**, and **5** exhibit splitting of the MLCT manifolds that arise from charge transfer from the Ru$^{\mathrm{II}}$ center to the bpy (eqn (5)) and N–N (eqn (6)) π^*-orbitals for the higher and lower energy transitions, respectively.[30] The energy difference between the MLCT transitions increases as the π^* acceptor ability of the N–N ligand increases.

$$[\mathrm{Ru^{II}(bpy)_2(N{-}N)}]^{2+}\ h\nu \rightarrow [\mathrm{Ru^{III}(bpy^{\bullet-})(bpy)(N{-}N)}]^{2+}* \tag{5}$$

$$[\mathrm{Ru^{II}(bpy)_2(N{-}N)}]^{2+}\ h\nu \rightarrow [\mathrm{Ru^{III}(bpy)_2(N{-}N^{\bullet-})}]^{2+}* \tag{6}$$

Photoinduced ligand ejection

The PCT photo-toxicity mechanism requires the loss of a ligand under illumination, in particular, a bidentate ligand for DNA metalation.[23,44,64,65] The rate constant for ligand dissociation (k_{pld}) for each complex was monitored using the apparatus shown in Fig. S3† with UV-vis spectra acquired at known time intervals during illumination with 467 nm light. The intensity of the light source was adjusted in accord with the molecule's molar absorptivities to generate an approximately equal number of excited states during photolysis (see

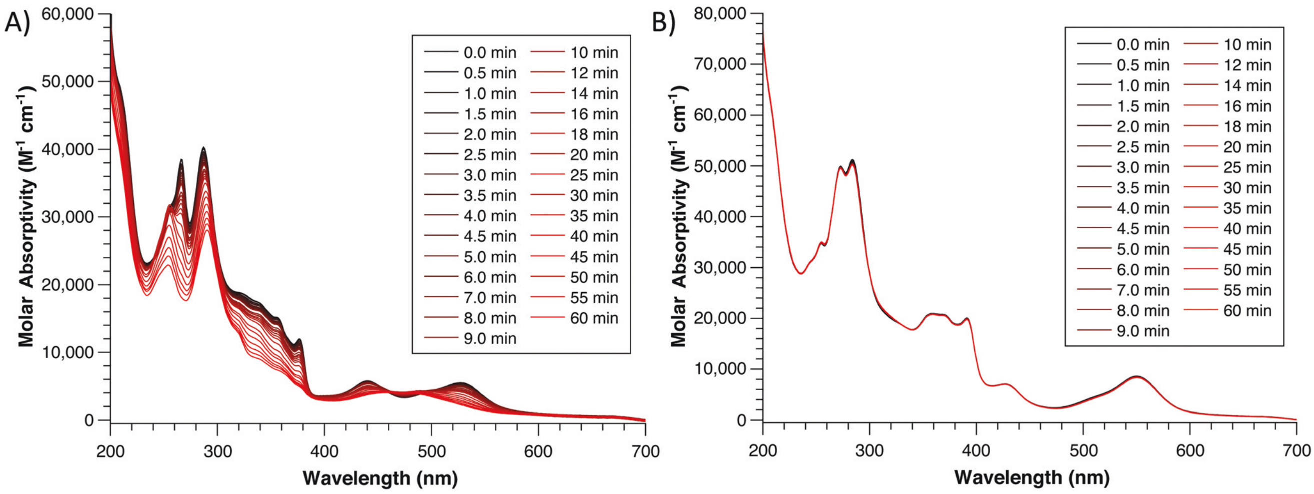

Fig. 5 Absorption spectra of complexes **3** (A) and **4** (B) in 3 mL H_2O monitored over time during irradiation with light from a Kessil PR160 (467 nm, 120 mW $\mathrm{cm^{-2}}$ at 5 cm). Light intensity was adjusted to correct for varying molar absorptivities at 467 nm (75% for **3** and 100% for **4**).

Table S1†). Representative UV-vis spectra of complexes **3** and **4** under illumination are shown in Fig. 5 with all of the spectra shown in the ESI (Fig. S4†).

As can be seen in Fig. 5 and Fig. S4,† only complex **3** undergoes a dramatic spectral change over the one hour of irradiation, including a decrease in intensity of the MLCT transition at 530 nm as well as the $\pi \rightarrow \pi^*$ transition from 320–380 nm. The resulting spectrum is in good agreement with the spectrum previously reported for $[\mathrm{Ru(bpy)_2(OH_2)_2}]^{2+}$.[23,66,67] Observations are consistent with the photoinduced ejection of the N–N ligand upon irradiation of **3** (eqn (7)).[23,68,69] All of the complexes were stable in solution in the dark for over a year (Fig. S5†).

$$[\mathrm{Ru^{II}(bpy)_2(L3)}]^{2+} + h\nu \rightarrow [\mathrm{Ru^{II}(bpy)_2(OH_2)_2}]^{2+} + \mathrm{L3} \qquad (7)$$

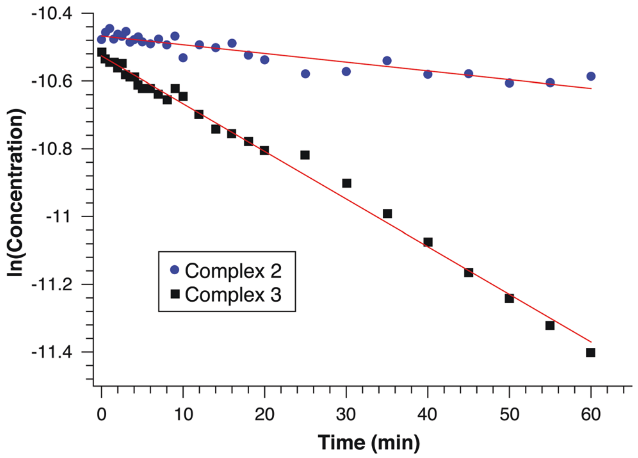

Fig. 6 First-order fits (red lines) for photoinduced ligand dissociation of ln(concentration) *versus* time for complexes **2** (blue) and **3** (black).

Of the remaining complexes, only **2** exhibits spectral changes under 467 nm illumination while **1**, **4**, and **5** are largely unperturbed (Fig. S4†). The kinetics for the photoinduced ligand ejection for **2** and **3** were fit to a first-order reaction equation (Fig. 6) with the rate constants (k_{pld}) being reported in Table 2. As expected, the increase in steric bulk resulted in increased k_{pld} in the order **1** ($\ll 10^{-6}$ s^{-1}) < **2** (4.3×10^{-5} s^{-1}) < **3** (2.3×10^{-4} s^{-1}). In contrast and unexpectedly, despite increased steric bulk around the Ru(II) center for **4** and **5**, which results in lowering the energy of the formally antibonding ^{3}dd* states that lead to ligand dissociation,[47,70,71] complexes **4** and **5** remained largely intact. To ensure lack of photoreactivity was not due to differences in molar absorptions the same experiments were conducted with a broad spectrum white-LED lamp, which showed the same general trends and relative differences in k_{pld} as described above (see Fig. S5†).

As first reported by Glazer and co-workers, and confirmed under the same conditions used here, $[\mathrm{Ru(bpy)_2(6,6'\text{-}dmb)}]^{2+}$ (where 6,6′-dmb = 6,6′-dimethyl-2,2′-bipyridine) undergoes complete ligand dissociation in under a minute of illumination (see Fig. S6†).[23] However, it should be noted that while the increased steric bulk in **3**, **4**, and **5** distorts the pseudo-octahedral around the Ru(II) center lowering the ^{3}dd* states, the introduction of non-coordinating electronegative heteroatoms in **4** and **5** also lower the N–N π^* orbitals and the energy of the ^{3}MLCT states.[30,47] This may result in the ligand dissociative ^{3}dd* states being inaccessible at room temperature, as will be discussed in the next section.

Emission spectroscopy

The steady-state and time-resolved emission for the complexes in H_2O were acquired under 445 nm excitation and the results

Table 2 Spectroscopic and ligand ejection properties for the complexes **1–5**

			Emission at rt[c]				
Compound	Absorbance[a] λ (nm) ($\varepsilon \times 10^3$ M^{-1} cm^{-1})	K_{pld}[b] (s^{-1})	$\lambda_{\max}$ (nm)	τ (ns)	ϕPL	k_r[d] ($\times 10^4$ s^{-1})	k_{nr}[e] ($\times 10^6$ s^{-1})
1	454 (11.6) 417 (8.7) 286 (69.9)	—	620	550	0.042	7.6	1.7
2	489 (6.2) 450 (7.6) 288 (46.2)	4.3×10^{-5}	710	195	0.006	2.9	4.9
3	527 (5.6) 440 (5.8) 287 (40.6)	2.3×10^{-4}	760	125	0.006	4.8	8.0
4	551 (8.6) 426 (7.1) 285 (51.2)	—	830[f]	13	—	—	—
5	564 (6.9) 404 (19.2) 279 (46.3)	—	850[f]	22	—	—	—

[a] Measured in H_2O. [b] Measured in H_2O utilizing the light from a Kessil PR160 (467 nm, 120 mW cm^{-2} at 5 cm) illuminated a quartz cuvette containing 3 mL of solutions of known concentration 5 cm away from the light source. Light intensity was adjusted to correct for varying molar absorptivities. [c] Emission data acquired using dilute solutions and lifetimes calculated from monoexponential fits. [d] $k_r = \phi/\tau$. [e] $k_{nr} = (1 - \phi)/\tau$. [f] Emission maxima from reference[30] as acquired in MeCN.

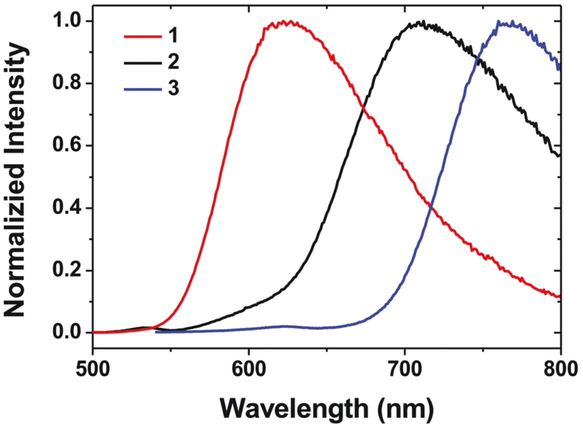

Fig. 7 Normalized emission spectra of **1**, **2** and **3** in N_2 deaerated H_2O (λ_{ex} = 445 nm).

are shown in Fig. 7 and summarized in Table 2. The maximum emission energy decreases in the order **1** (620 nm) > **2** (710 nm) > **3** (760 nm). Due to instrument limitations (*i.e.*, low signal beyond 800 nm), we were unable to determine emission maxima for **4** and **5** in H_2O (see Fig. S7 and S8†). However, the emission onset was similar to that previously reported for **4** and **5** in MeCN (830 and 850 nm, respectively),[30] consequently those values were included in Table 2 and used for further analysis.

Previous analyses have shown a linear relationship between the electrochemical gap $\Delta E_{1/2}$, (*i.e.*, $\Delta E_{1/2} = E_{1/2}(\text{Ru}^{3+/2+}) - E_{1/2}(\text{Ru}^{2+/+})$) and the absorption/emission maxima of ruthenium(II) polypyridyl complexes.[48,57,72,73] Fig. 8 presents how the lowest energy absorption ($\bar{\nu}_{abs}$) and emission ($\bar{\nu}_{em}$) maxima vary with $\Delta E_{1/2}$. Both absorption and emission energies exhibit a linear relationship with $\Delta E_{1/2}$, expected for transitions to and from MLCT excited states.[48,72,74]

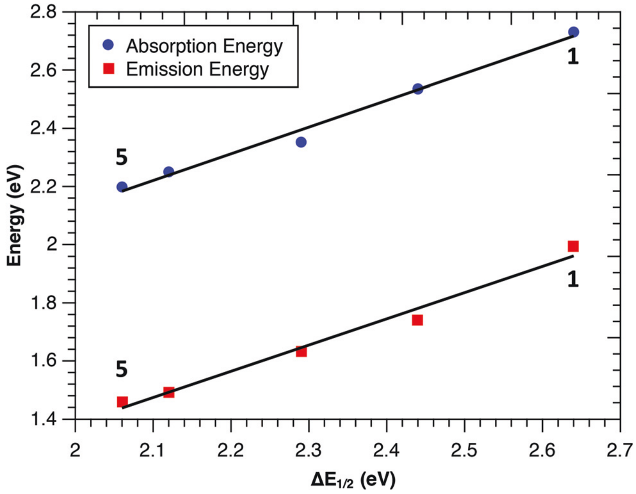

Fig. 8 Variation of absorption (blue circle), and emission (red squares) maximum energies with the electrochemical gap ($\Delta E_{1/2} = E_{1/2}(\text{Ru}^{3+/2+}) - E_{1/2}(\text{Ru}^{2+/+})$ for complexes **1–5** (right-to-left) in H_2O. Note that emission energies for complexes **4** and **5** are from reported values.[30]

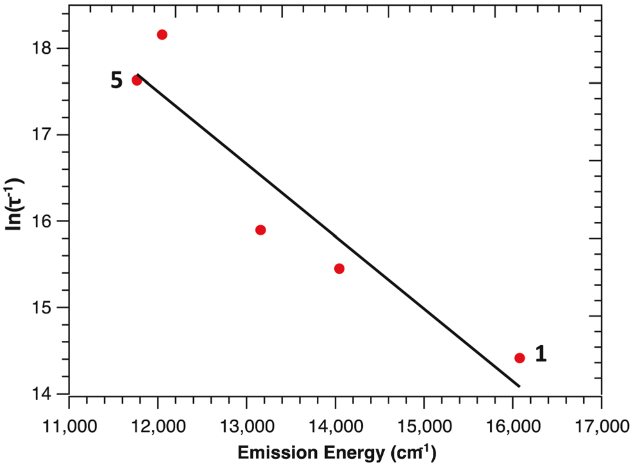

Fig. 9 Plot of emission energy *vs.* ln τ^{-1} for complexes **1–5** (right-to-left) in H_2O at 25 °C.

Time-resolved emission kinetics were monitored at the emission peak maxima for **1–3** and at 800 nm for **4–5**. The emission decays were fit with a singlet exponential function and the results are summarized in Table 2. The emission lifetime decreased in the order **1** (550 ns) > **2** (195 ns) > **3** (125 ns) > **4** (13 ns) ≈ **5** (22 ns). The approximately linear relationship between the excited state lifetime and maximum emission energy is in good agreement with that expected by the energy gap law (Fig. 9).[75]

Temperature dependent emission

As noted above, ligand dissociation for ruthenium(II) polypyridyl complexes is typically attributed to thermal population of the formally antibonding metal-centered ^{3}dd* state from the ^{3}MLCT* manifold.[71,75] Temperature-dependent emission lifetime measurements is a strategy that can be used to determine the activation energy barrier (ΔE_{pld}, energy gap for photo-induced ligand dissociation) between the ^{3}MLCT* and ^{3}dd* states.[52] Here we monitored changes in the excited state lifetime of **1–3** with respect to temperature with example decay curves show in Fig. 10 for **1** and temperature dependent lifetimes summarized in Fig. 11 (all emission decays are shown in Fig. S9–S11†).

As expected, the excited state lifetime of all complexes decreases with increasing temperature. The results were then fit with eqn (8) where $\tau(T)$ is the lifetime at a given temperature (T), R is the ideal gas constant, k^0 is a pre-exponential factor, and k is the sum of radiative and non-radiative decay rates ($k = k_r + k_{nr}$).[52] The results of the fitting are summarized in Table 3.

$$\frac{1}{\tau(T)} = k + k^0 \exp[-(\Delta E_{pld}/RT)] \tag{8}$$

The energy gap, ΔE_{pld}, of $[\text{Ru(bpy)}_3]^{2+}$ (**1**) of 2580 cm^{-1} is in reasonable agreement with those previously obtained for **1** in aqueous conditions, where ΔE_{pld} is attributed to the thermal

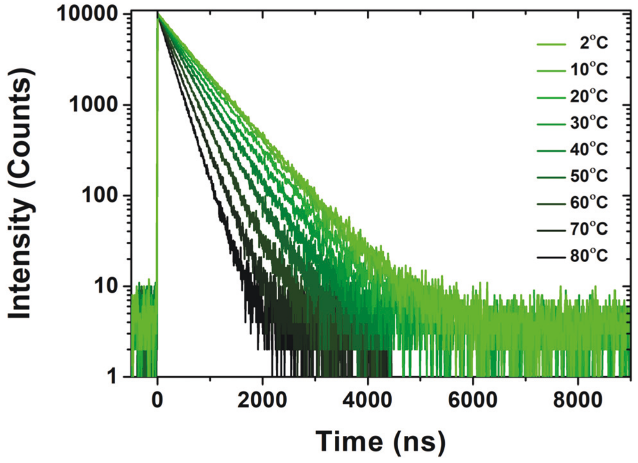

Fig. 10 Emission decays for **1** in N_2 deaerated H_2O at various temperatures (λ_{ex} = 405 nm, λ_{em} = emission maximum).

Table 3 Fitting parameters for the temperature dependent emission kinetics for **1–3** in N_2 deaerated H_2O

Sample	k ($\times 10^6$ s^{-1})	k^0	ΔE_{pld} (cm^{-1})
1	1.4	1.1×10^{11}	2580
2	2.8	3.0×10^{8}	1000
3	5.8	1.5×10^{8}	850

barrier of excited-state deactivation *via* metal centered ^{3}dd* states.[76] The ΔE_{pld} for the complexes measured here decreases in the order **1** (2580 cm^{-1}) > **2** (1000 cm^{-1}) > **3** (850 cm^{-1}), which correlates with the trend of decreasing lifetime. This trend in ΔE_{pld} also inversely correlates with the increasing rate constant for photoinduced ligand ejection, k_{pld}, in the order **3** > **2** ≫ **1**, further reinforcing the hypothesis that population of the ^{3}dd* states is responsible for ligand dissociation. It should also be noted that ligand dissociation from the ^{3}dd* state is rapid compared to relaxation back to the MLCT manifold and/or ground state.[48,52,77] Consequently, the more than 1000 cm^{-1} greater ΔE_{pld} is responsible for the increased stability and lack of ligand dissociation for **1**, as compared to **2** and **3**. Unfortunately, due to their short lifetimes and our limited detector response, attempts to measure temperature dependent lifetimes for **4** and **5** under the same conditions were unsuccessful. The importance in the observed variation of ΔE_{pld} energies and PCT design will be discussed below.

Cytotoxicity assays

MTT (3-[4,5-dimethylthiazol-2-yl]-2,5 diphenyl tetrazolium bromide) dye reduction assays were used to analyze the potential biological activity of complexes **1–5** against human embryonic kidney (HEK293T) cell cultures (Fig. S12†) with and without illumination. Briefly, HEK293T cells were seeded into 96-well plate and dosed with varying concentrations of the complexes. The cultures were then either exposed to 467 nm

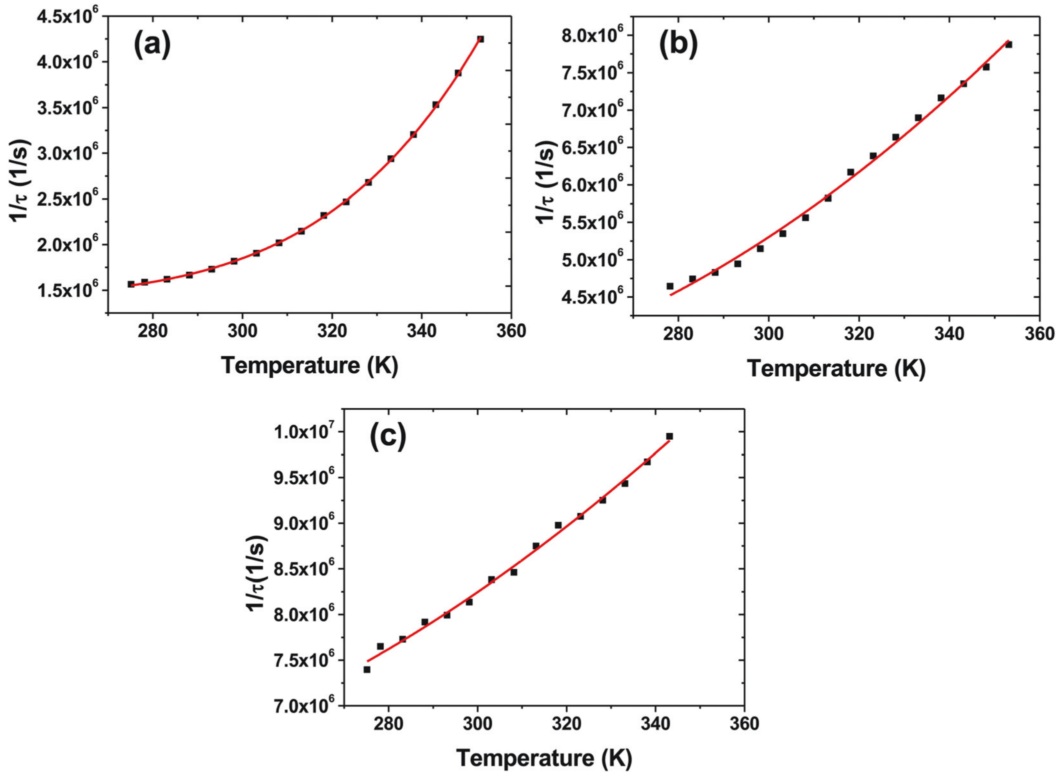

Fig. 11 Plot of *1/τ versus* temperature for complexes **1** (a), **2** (b) and **3** (c) in N_2 deaerated H_2O.

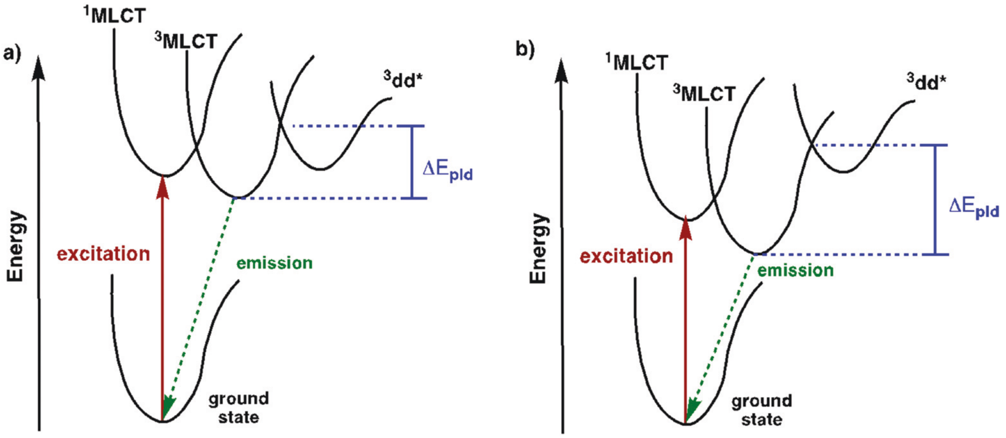

Fig. 12 Excited state diagrams of ruthenium polypyridyl compounds for complexes that absorb at shorter wavelengths (a, such as **3**) compared to longer wavelengths (b, such as **4**).

illumination for 60 minutes, or covered from irradiation *in situ* (see ESI† for full experimental details). Overall, as might be expected from the outcomes above, the complexes displayed relatively low cytotoxicity with or without illumination. However, all of the complexes except for **2** displayed statistically significant increased cytotoxicity under illumination compared to non-irradiated samples at the 200 μM concentration (Fig. S12†). Control experiments with HEK293T cells, with and without illumination, showed no light dependence with cisplatin and a significant dependence with $[Ru(bpy)_2(6,6'\text{-dmb})]^{2+}$, as expected (see Fig. S14†).

Due to concerns of overheating the samples and causing cell death, all cytotoxicity studies under illumination were carried out at 25% of the 467 nm lamp intensity. As a result, to correct for variations in absorptivity of the complexes at 467 nm, the difference in cell viability between illuminated and non-illuminated samples were divided by their molar absorptivities (Table S1†) to give a comparison between the complexes (Fig. S13†). As expected, **3** had the highest photoinduced cytotoxic behavior, however unexpectedly, **5** showed the second highest when correcting for these absorptivity differences. While these results demonstrate the ability of the complexes to act as phototoxic agents, further studies are needed to better understand their cytotoxic behavior, in addition to designing new and more active compounds based upon the discussion given below.

Balancing absorption in therapeutic window and ligand ejection

As has been previously discussed, current PCTs suffer from minimal absorption within the 'therapeutic window' to be candidates for clinical oncology use. Given the understanding of Ru(II) polypyridyl light absorption and photophysics, we set out to design a new series of PCTs that incorporated increased conjugation and/or electronegative heteroatoms to shift the absorption closer to the therapeutic window. At the same time, the series also introduced steric bulk around the metal center to promote photoinduced ligand ejection, a key step in the cytotoxicity mechanism. However, as demonstrated here and poignantly exemplified with complexes **3** and **4**, one must strike a balance between shifting absorptions to longer wavelengths and the accessibility of the dissociative ^{3}dd* excited states. As shown in Fig. 5, **3** undergoes ligand loss under 467 nm illumination with a first-order rate constant of 2.3×10^{-4} s^{-1} where **4** shows no measurable dissociation. Sterically, there is little to no difference in the ligands, suggesting that the dissociative ^{3}dd* state is at the same relative energy in both. However, the introduction of a single electronegative heteroatom to the periphery of **4** resulted in a lowering of ^{1}MLCT excitation by 0.10 eV (527 nm for **3** and 551 nm for **4**) and ^{3}MLCT emission by 0.14 eV (760 nm for **3** and 830 nm for **4**). As a result of lowering the MLCT* states, ΔE_{pld} increases for **4** compared to **3** (see Fig. 12). This makes the dissociative ^{3}dd* states inaccessible at room temperature for **4**, ultimately inhibiting photoinduced ligand ejection.

These findings demonstrate that in the pursuit of complexes designed to act as PCTs one must closely consider the excited-state manifolds and the effect shifting energies can have on the ability of the compound to act as a phototoxic agent. In the series of compounds reported herein, the introduction of a single electronegative heteroatom shut off the cytotoxicity of the complex, despite significant strain around the metal center. These understandings will aid in the future design of PCTs to help strike a balance between therapeutic window absorption, thermal stability, and photoactivation kinetics that is critical for successful clinical adoption of PCTs.

Conclusions

We have described here the synthesis, characterization, spectrochemical, and photophysical analysis of a series of ruthenium(II) polypyridyl complexes of the type $[Ru(bpy)_2(N\text{–}N)]^{2+}$

designed to be used as PCTs. The N–N bidentate ligands were selected to introduce increased conjugation and/or electronegative heteroatom to lower the π*-acceptor levels. Through the series, the lowest energy MLCT absorption maximum was red-shifted from **1** ($\lambda_{\max}$ = 454 nm) to **5** ($\lambda_{\max}$ = 564 nm). However, despite increased steric bulk, photolysis experiments only showed appreciable photoinduced ligand dissociation for complexes **2** (k_{pld} = 4.3 × 10^{-5}) and **3** (k_{pld} = 2.3 × 10^{-4}). Time-resolved and temperature-dependent emission studies revealed that lowering π*-acceptor energy levels in the N–N ligands decreased emission energies ($\lambda_{\max}$ = 620 nm for **1** to $\lambda_{\max}$ = 850 nm for **5**) and increased the energy barrier (ΔE_{pld}, 2580 cm^{-1} for **1** and 850 cm^{-1} for **3**) to access the dissociated ^{3}dd* states. This demonstrates a balancing act between red-shifting the MLCT absorption into the 'therapeutic window' while still maintaining photoinduced ligand ejection at room temperature which can be applied to future PCT design.

Author contributions

ABM, NPV, TMF, APC, VMD, and DLA performed the synthesis, full characterization, and photostability studies of the reported complexes. JC performed the photophysical analysis of the complexes and QQ and SMS performed the cytotoxicity analyses. ABM, KH, and DLA did majority of the writing-original draft work with JC and SMS writing the emission and cytotoxicity sections, respectively. Brittany Gentry and Michaela Hall also assisted in the cytotoxicity studies. DLA performed the conceptualization and writing-review & editing work.

Conflicts of interest

There are no conflicts to declare.

Acknowledgements

This work was supported by the Arthur Vining David Foundations under Grant No. G-1808-18898, East Tennessee Foundation Youth Endowment Grant No. 21992, and Eastman Chemical Company supporting A. B. M, N. P. V., T. M. F., A. P. C., V. M. D., and D. L. A. Photophysical measurements were supported by the National Science Foundation under Grant No. DMR-1752782 supporting J. C. and K. H. Cytotoxicity measurements were completed by Q. Q. and S. M. S. Mass spectrometric analyses were performed at the University of Tennessee, Knoxville Biological and Small Molecule Mass Spectrometry Core with the assistance of Dr Shawn R. Campagna, Dr Hector F. Castro, and Vernon Stafford.

References

1 R. Paprocka, M. Wiese-Szadkowska, S. Janciauskiene, T. Kosmalski, M. Kulik and A. Helmin-Basa, Latest developments in metal complexes as anticancer agents, *Coord. Chem. Rev.*, 2022, **452**, 214307.

2 L. Gourdon, K. Cariou and G. Gasser, Phototherapeutic anticancer strategies with first-row transition metal complexes: a critical review, *Chem. Soc. Rev.*, 2022, **51**(3), 1167–1195.

3 R. L. Siegel, K. D. Miller and A. Jemal, Cancer statistics, 2020, *CA-Cancer J. Clin.*, 2020, **70**(1), 7–30.

4 A. C. Society, Global Cancer Facts & Figures (accessed 9/23/2021).

5 M. Galanski, M. A. Jakupec and B. K. Keppler, Update of the preclinical situation of anticancer platinum complexes: novel design strategies and innovative analytical approaches, *Curr. Med. Chem.*, 2005, **12**(18), 2075–2094.

6 T. C. Johnstone, G. Y. Park and S. J. Lippard, Understanding and Improving Platinum Anticancer Drugs – Phenanthriplatin, *Anticancer Res.*, 2014, **34**(1), 471–476.

7 P. Mistry, L. R. Kelland, G. Abel, S. Sidhar and K. R. Harrap, The relationships between glutathione, glutathione-S-transferase and cytotoxicity of platinum drugs and melphalan in eight human ovarian carcinoma cell lines, *Br. J. Cancer*, 1991, **64**(2), 215.

8 L. Kelland, The resurgence of platinum-based cancer chemotherapy, *Nat. Rev. Cancer*, 2007, **7**(8), 573.

9 P. Yang, J. O. Ebbert, Z. Sun and R. M. Weinshilboum, Role of the glutathione metabolic pathway in lung cancer treatment and prognosis: a review, *J. Clin. Oncol.*, 2006, **24**(11), 1761–1769.

10 J. Shi, P. W. Kantoff, R. Wooster and O. C. Farokhzad, Cancer nanomedicine: progress, challenges and opportunities, *Nat. Rev. Cancer*, 2017, **17**(1), 20.

11 S. Monro, K. L. Colón, H. Yin, J. Roque, P. Konda, S. Gujar, R. P. Thummel, L. Lilge, C. G. Cameron and S. A. McFarland, Transition Metal Complexes and Photodynamic Therapy from a Tumor-Centered Approach: Challenges, Opportunities, and Highlights from the Development of TLD1433, *Chem. Rev.*, 2019, **119**(2), 797–828.

12 C. Imberti, P. Zhang, H. Huang and P. J. Sadler, New Designs for Phototherapeutic Transition Metal Complexes, *Angew. Chem., Int. Ed.*, 2020, **59**(1), 61–73.

13 F. Heinemann, J. Karges and G. Gasser, Critical Overview of the Use of Ru(II) Polypyridyl Complexes as Photosensitizers in One-Photon and Two-Photon Photodynamic Therapy, *Acc. Chem. Res.*, 2017, **50**(11), 2727–2736.

14 Y. Zhang, Q. Zhou, N. Tian, C. Li and X. Wang, Ru(II)-Complex-Based DNA Photocleaver Having Intense Absorption in the Phototherapeutic Window, *Inorg. Chem.*, 2017, **56**(4), 1865–1873.

15 M. T. Jarvi, M. S. Patterson and B. C. Wilson, Insights into photodynamic therapy dosimetry: simultaneous singlet oxygen luminescence and photosensitizer photobleaching measurements, *Biophys. J.*, 2012, **102**(3), 661–671.

16 S. Clement, W. Deng, E. Camilleri, B. C. Wilson and E. M. Goldys, X-ray induced singlet oxygen generation by nanoparticle-photosensitizer conjugates for photodynamic

therapy: determination of singlet oxygen quantum yield, *Sci. Rep.*, 2016, **6**(1), 19954.

17 R. A. Weersink, A. Bogaards, M. Gertner, S. R. H. Davidson, K. Zhang, G. Netchev, J. Trachtenberg and B. C. Wilson, Techniques for delivery and monitoring of TOOKAD (WST09)-mediated photodynamic therapy of the prostate: Clinical experience and practicalities, *J. Photochem. Photobiol., B*, 2005, **79**(3), 211–222.

18 L. Kohler, L. Nease, P. Vo, J. Garofolo, D. K. Heidary, R. P. Thummel and E. C. Glazer, Photochemical and Photobiological Activity of Ru(II) Homoleptic and Heteroleptic Complexes Containing Methylated Bipyridyl-type Ligands, *Inorg. Chem.*, 2017, **56**(20), 12214–12223.

19 C. Griffith, A. S. Dayoub, T. Jaranatne, N. Alatrash, A. Mohamedi, K. Abayan, Z. S. Breitbach, D. W. Armstrong and F. M. MacDonnell, Cellular and cell-free studies of catalytic DNA cleavage by ruthenium polypyridyl complexes containing redox-active intercalating ligands, *Chem. Sci.*, 2017, **8**(5), 3726–3740.

20 A. Yadav, T. Janaratne, A. Krishnan, S. S. Singhal, S. Yadav, A. S. Dayoub, D. L. Hawkins, S. Awasthi and F. M. MacDonnell, Regression of lung cancer by hypoxia-sensitizing ruthenium polypyridyl complexes, *Mol. Cancer Ther.*, 2013, **12**(5), 643–653.

21 S. J. Steinke, S. Gupta, E. J. Piechota, C. E. Moore, J. J. Kodanko and C. Turro, Photocytotoxicity and photo-induced phosphine ligand exchange in a Ru(ii) polypyridyl complex, *Chem. Sci.*, 2022, **13**(7), 1933–1945.

22 K. König, Multiphoton microscopy in life sciences, *J. Microsc.*, 2000, **200**(Pt 2), 83–104.

23 B. S. Howerton, D. K. Heidary and E. C. Glazer, Strained Ruthenium Complexes Are Potent Light-Activated Anticancer Agents, *J. Am. Chem. Soc.*, 2012, **134**(20), 8324–8327.

24 K. Arora, M. Herroon, M. H. Al-Afyouni, N. P. Toupin, T. N. Rohrabaugh, L. M. Loftus, I. Podgorski, C. Turro and J. J. Kodanko, Catch and Release Photosensitizers: Combining Dual-Action Ruthenium Complexes with Protease Inactivation for Targeting Invasive Cancers, *J. Am. Chem. Soc.*, 2018, **140**(43), 14367–14380.

25 M. H. Al-Afyouni, T. N. Rohrabaugh, K. F. Al-Afyouni and C. Turro, New Ru(ii) photocages operative with near-IR light: new platform for drug delivery in the PDT window, *Chem. Sci.*, 2018, **9**(32), 6711–6720.

26 D. Havrylyuk, D. K. Heidary, Y. Sun, S. Parkin and E. C. Glazer, Photochemical and Photobiological Properties of Pyridyl-pyrazol(in)e-Based Ruthenium(II) Complexes with Sub-micromolar Cytotoxicity for Phototherapy, *ACS Omega*, 2020, **5**(30), 18894–18906.

27 H. Shi, C. Imberti and P. J. Sadler, Diazido platinum(IV) complexes for photoactivated anticancer chemotherapy, *Inorg. Chem. Front.*, 2019, **6**(7), 1623–1638.

28 V. H. S. van Rixel, V. Ramu, A. B. Auyeung, N. Beztsinna, D. Y. Leger, L. N. Lameijer, S. T. Hilt, S. E. Le Dévédec, T. Yildiz, T. Betancourt, M. B. Gildner, T. W. Hudnall, V. Sol, B. Liagre, A. Kornienko and S. Bonnet, Photo-Uncaging of a Microtubule-Targeted Rigidin Analogue in Hypoxic Cancer Cells and in a Xenograft Mouse Model, *J. Am. Chem. Soc.*, 2019, **141**(46), 18444–18454.

29 A. C. Hachey, D. Havrylyuk and E. C. Glazer, Biological activities of polypyridyl-type ligands: implications for bio-inorganic chemistry and light-activated metal complexes, *Curr. Opin. Chem. Biol.*, 2021, **61**, 191–202.

30 D. L. Ashford, C. R. K. Glasson, M. R. Norris, K. Hanson, J. J. Concepcion, S. Keinan, M. K. Brennaman, J. L. Templeton and T. J. Meyer, Controlling Ground and Excited State Properties through Ligand Changes in Ruthenium Polypyridyl Complexes, *Inorg. Chem.*, 2014, **53**(11), 5637–5646.

31 C. Reichardt, S. Monro, F. H. Sobotta, K. L. Colón, T. Sainuddin, M. Stephenson, E. Sampson, J. Roque, H. Yin, J. C. Brendel, C. G. Cameron, S. McFarland and B. Dietzek, Predictive Strength of Photophysical Measurements for in Vitro Photobiological Activity in a Series of Ru(II) Polypyridyl Complexes Derived from π-Extended Ligands, *Inorg. Chem.*, 2019, **58**(5), 3156–3166.

32 J. Fong, K. Kasimova, Y. Arenas, P. Kaspler, S. Lazic, A. Mandel and L. Lilge, A novel class of ruthenium-based photosensitizers effectively kills in vitro cancer cells and in vivo tumors, *Photochem. Photobiol. Sci.*, 2015, **14**(11), 2014–2023.

33 S. Monro, K. L. Colon, H. Yin, J. Roque 3rd, P. Konda, S. Gujar, R. P. Thummel, L. Lilge, C. G. Cameron and S. A. McFarland, Transition Metal Complexes and Photodynamic Therapy from a Tumor-Centered Approach: Challenges, Opportunities, and Highlights from the Development of TLD1433, *Chem. Rev.*, 2019, **119**(2), 797–828.

34 D. W. Thompson, A. Ito and T. J. Meyer, [Ru(bpy)3]2+* and other remarkable metal-to-ligand charge transfer (MLCT) excited states, *Pure Appl. Chem.*, 2013, **85**(7), 1257–1305.

35 J. N. Demas and A. W. Adamson, Tris (2,2′-bipyridine)ruthenium(II) sensitized reactions of some oxalato complexes, *J. Am. Chem. Soc.*, 1973, **95**(16), 5159–5168.

36 C. R. Bock, T. J. Meyer and D. G. Whitten, Electron transfer quenching of the luminescent excited state of tris(2,2′-bipyridine)ruthenium(II). Flash photolysis relaxation technique for measuring the rates of very rapid electron transfer reactions, *J. Am. Chem. Soc.*, 1974, **96**(14), 4710–4712.

37 L. N. Lameijer, D. Ernst, S. L. Hopkins, M. S. Meijer, S. H. C. Askes, S. E. Le Dévédec and S. Bonnet, A Red-Light-Activated Ruthenium-Caged NAMPT Inhibitor Remains Phototoxic in Hypoxic Cancer Cells, *Angew. Chem., Int. Ed.*, 2017, **56**(38), 11549–11553.

38 T. Respondek, R. N. Garner, M. K. Herroon, I. Podgorski, C. Turro and J. J. Kodanko, Light Activation of a Cysteine Protease Inhibitor: Caging of a Peptidomimetic Nitrile with RuII(bpy)2, *J. Am. Chem. Soc.*, 2011, **133**(43), 17164–17167.

39 A. Zamora, C. A. Denning, D. K. Heidary, E. Wachter, L. A. Nease, J. Ruiz and E. C. Glazer, Ruthenium-containing P450 inhibitors for dual enzyme inhibition and DNA damage, *Dalton Trans.*, 2017, **46**(7), 2165–2173.

40 J. Karges, F. Heinemann, M. Jakubaszek, F. Maschietto, C. Subecz, M. Dotou, R. Vinck, O. Blacque, M. Tharaud, B. Goud, E. Viñuelas Zahínos, B. Spingler, I. Ciofini and G. Gasser, Rationally Designed Long-Wavelength Absorbing Ru(II) Polypyridyl Complexes as Photosensitizers for Photodynamic Therapy, *J. Am. Chem. Soc.*, 2020, **142**(14), 6578–6587.

41 A. Li, R. Yadav, J. K. White, M. K. Herroon, B. P. Callahan, I. Podgorski, C. Turro, E. E. Scott and J. J. Kodanko, Illuminating cytochrome P450 binding: Ru(ii)-caged inhibitors of CYP17A1, *Chem. Commun.*, 2017, **53**(26), 3673–3676.

42 H. D. Cole, J. A. Roque 3rd, L. M. Lifshits, R. Hodges, P. C. Barrett, D. Havrylyuk, D. Heidary, E. Ramasamy, C. G. Cameron, E. C. Glazer and S. A. McFarland, Fine-Feature Modifications to Strained Ruthenium Complexes Radically Alter Their Hypoxic Anticancer Activity(dagger), *Photochem. Photobiol.*, 2022, **98**(1), 73–84.

43 E. Wachter, A. Zamora, D. K. Heidary, J. Ruiz and E. C. Glazer, Geometry matters: inverse cytotoxic relationship for cis/trans-Ru(ii) polypyridyl complexes from cis/trans-[PtCl2(NH3)2], *Chem. Commun.*, 2016, **52**(66), 10121–10124.

44 E. Wachter, D. K. Heidary, B. S. Howerton, S. Parkin and E. C. Glazer, Light-activated ruthenium complexes photobind DNA and are cytotoxic in the photodynamic therapy window, *Chem. Commun.*, 2012, **48**(77), 9649–9651.

45 L. M. Loftus, K. F. Al-Afyouni and C. A.-O. h. o. o. Turro, New Ru(II) Scaffold for Photoinduced Ligand Release with Red Light in the Photodynamic Therapy (PDT) Window. (1521–3765 (Electronic)).

46 M. S. Meijer, M. M. Natile and S. Bonnet, 796 nm Activation of a Photocleavable Ruthenium(II) Complex Conjugated to an Upconverting Nanoparticle through Two Phosphonate Groups, *Inorg. Chem.*, 2020, **59**(20), 14807–14818.

47 J. D. Knoll, B. A. Albani and C. Turro, Excited state investigation of a new Ru(II) complex for dual reactivity with low energy light, *Chem. Commun.*, 2015, **51**(42), 8777–8780.

48 J. V. Caspar and T. J. Meyer, Photochemistry of MLCT excited states. Effect of nonchromophoric ligand variations on photophysical properties in the series cis-Ru(bpy)2L22+, *Inorg. Chem.*, 1983, **22**(17), 2444–2453.

49 B. Durham, J. V. Caspar, J. K. Nagle and T. J. Meyer, Photochemistry of tris(2,2′-bipyridine)ruthenium(2+) ion, *J. Am. Chem. Soc.*, 1982, **104**(18), 4803–4810.

50 P. A. Anderson, G. F. Strouse, J. A. Treadway, F. R. Keene and T. J. Meyer, Black MLCT Absorbers, *Inorg. Chem.*, 1994, **33**(18), 3863–3864.

51 P. A. Anderson, F. R. Keene, T. J. Meyer, J. A. Moss, G. F. Strouse and J. A. Treadway, Manipulating the properties of MLCT excited states, *J. Chem. Soc., Dalton Trans. (1972-1999)*, 2002, (20), 3820–3831.

52 J. V. Caspar and T. J. Meyer, Photochemistry of tris(2,2′-bipyridine)ruthenium(2+) ion (Ru(bpy)32+). Solvent effects, *J. Am. Chem. Soc.*, 1983, **105**(17), 5583–5590.

53 F. Qu, R. W. Lamb, C. G. Cameron, S. Park, O. Oladipupo, J. L. Gray, Y. Xu, H. D. Cole, M. Bonizzoni, Y. Kim, S. A. McFarland, C. E. Webster and E. T. Papish, Singlet Oxygen Formation *vs.* Photodissociation for Light-Responsive Protic Ruthenium Anticancer Compounds: The Oxygenated Substituent Determines Which Pathway Dominates, *Inorg. Chem.*, 2021, **60**(4), 2138–2148.

54 N. Leblanc, S. Sproules, K. Fink, L. Sanguinet, O. Alévêque, E. Levillain, P. Rosa and A. K. Powell, A fascinating multifaceted redox-active chelating ligand: introducing the N,N′-dimethyl-3,3′-biquinoxalinium "methylbiquinoxen" platform, *Chem. Sci.*, 2016, **7**(6), 3820–3828.

55 M. R. Norris, J. J. Concepcion, C. R. K. Glasson, Z. Fang, A. M. Lapides, D. L. Ashford, J. L. Templeton and T. J. Meyer, Synthesis of Phosphonic Acid-Derivatized Bipyridine Ligands and Their Ruthenium Complexes, *Inorg. Chem.*, 2013, **52**(21), 12492–12501.

56 J. Gu, J. Chen and R. H. Schmehl, Using Intramolecular Energy Transfer to Transform non-Photoactive, Visible-Light-Absorbing Chromophores into Sensitizers for Photoredox Reactions, *J. Am. Chem. Soc.*, 2010, **132**(21), 7338–7346.

57 A. B. P. Lever, Electrochemical parametrization of metal complex redox potentials, using the ruthenium(III)/ruthenium(II) couple to generate a ligand electrochemical series, *Inorg. Chem.*, 1990, **29**(6), 1271–1285.

58 V. W.-W. Yam, V. W.-M. Lee, F. Ke and K.-W. M. Siu, Synthesis, Photophysics, and Electrochemistry of Ruthenium(II) Polypyridine Complexes with Crown Ether Pendants, *Inorg. Chem.*, 1997, **36**(10), 2124–2129.

59 D. P. Rillema and K. B. Mack, The low-lying excited state in ligand π-donor complexes of ruthenium(II): mononuclear and binuclear species, *Inorg. Chem.*, 1982, **21**(10), 3849–3854.

60 M. N. Ackermann and L. V. Interrante, Ruthenium(II) complexes of modified 1,10-phenanthrolines. 1. Synthesis and properties of complexes containing dipyridophenazines and a dicyanomethylene-substituted 1,10-phenanthroline, *Inorg. Chem.*, 1984, **23**(24), 3904–3911.

61 F. S. Saleh, M. R. Rahman, T. Okajima, L. Mao and T. Ohsaka, Determination of formal potential of NADH/NAD+ redox couple and catalytic oxidation of NADH using poly(phenosafranin)-modified carbon electrodes, *Bioelectrochemistry*, 2011, **80**(2), 121–127.

62 K. Khazim, D. Giustarini, R. Rossi, D. Verkaik, J. E. Cornell, S. E. D. Cunningham, M. Mohammad, K. Trochta, C. Lorenzo, F. Folli, S. Bansal and P. Fanti, Glutathione redox potential is low and glutathionylated and cysteinylated hemoglobin levels are elevated in maintenance hemodialysis patients, *Transl. Res.*, 2013, **162**(1), 16–25.

63 J. V. Caspar, E. M. Kober, B. P. Sullivan and T. J. Meyer, Application of the energy gap law to the decay of charge-transfer excited states, *J. Am. Chem. Soc.*, 1982, **104**(2), 630–632.

64 J. K. White, R. H. Schmehl and C. Turro, An overview of photosubstitution reactions of Ru(II) imine complexes and their application in photobiology and photodynamic therapy, *Inorg. Chim. Acta*, 2017, **454**, 7–20.

65 T. N. Singh and C. Turro, Photoinitiated DNA Binding by cis-[Ru(bpy)2(NH3)2]2+, *Inorg. Chem.*, 2004, **43**(23), 7260–7262.

66 B. Durham, S. R. Wilson, D. J. Hodgson and T. J. Meyer, Cis-trans photoisomerization in Ru(bpy)2(OH2)22+. Crystal structure of trans-[Ru(bpy)2(OH2)(OH)](ClO4)2, *J. Am. Chem. Soc.*, 1980, **102**(2), 600–607.

67 M. L. Gama Sauaia, E. Tfouni, R. Helena de Almeida Santos, M. Teresa do Prado Gambardella, M. P. F. M. Del Lama, L. Fernando Guimarães and R. Santana da Silva, Use of HPLC in the identification of cis and trans-diaquabis (2,2′-bipyridine)ruthenium(II) complexes: crystal structure of cis-[Ru(H_2O)2(bpy)2](PF6)2, *Inorg. Chem. Commun.*, 2003, **6**(7), 864–868.

68 A. N. Hidayatullah, E. Wachter, D. K. Heidary, S. Parkin and E. C. Glazer, Photoactive Ru(II) Complexes With Dioxinophenanthroline Ligands Are Potent Cytotoxic Agents, *Inorg. Chem.*, 2014, **53**(19), 10030–10032.

69 E. Wachter and E. C. Glazer, Mechanistic Study on the Photochemical "Light Switch" Behavior of [Ru(bpy) 2dmdppz]2+, *J. Phys. Chem. A*, 2014, **118**(45), 10474–10486.

70 Q. Sun, S. Mosquera-Vazquez, Y. Suffren, J. Hankache, N. Amstutz, L. M. Lawson Daku, E. Vauthey and A. Hauser, On the role of ligand-field states for the photophysical properties of ruthenium(II) polypyridyl complexes, *Coord. Chem. Rev.*, 2015, **282–283**, 87–99.

71 Q. Sun, S. Mosquera-Vazquez, L. M. Lawson Daku, L. Guénée, H. A. Goodwin, E. Vauthey and A. Hauser, Experimental Evidence of Ultrafast Quenching of the 3MLCT Luminescence in Ruthenium(II) Tris-bipyridyl Complexes via a 3dd State, *J. Am. Chem. Soc.*, 2013, **135**(37), 13660–13663.

72 J. Li, P. I. Djurovich, B. D. Alleyne, M. Yousufuddin, N. N. Ho, J. C. Thomas, J. C. Peters, R. Bau and M. E. Thompson, Synthetic Control of Excited-State Properties in Cyclometalated Ir(III) Complexes Using Ancillary Ligands, *Inorg. Chem.*, 2005, **44**(6), 1713–1727.

73 S. I. Gorelsky, E. S. Dodsworth, A. B. P. Lever and A. A. Vlcek, Trends in metal-ligand orbital mixing in generic series of ruthenium N-donor ligand complexes - effect on electronic spectra and redox properties, *Coord. Chem. Rev.*, 1998, **174**, 469–494.

74 E. M. Kober, J. L. Marshall, W. J. Dressick, B. P. Sullivan, J. V. Caspar and T. J. Meyer, Synthetic control of excited states. Nonchromophoric ligand variations in polypyridyl complexes of osmium(II), *Inorg. Chem.*, 1985, **24**(18), 2755–2763.

75 J. Jortner, Radiationless transitions, *Pure Appl. Chem.*, 1971, **27**(3), 389–420.

76 J. Van Houten and R. J. Watts, Temperature dependence of the photophysical and photochemical properties of the tris (2,2′-bipyridyl)ruthenium(II) ion in aqueous solution, *J. Am. Chem. Soc.*, 1976, **98**(16), 4853–4858.

77 D. W. Thompson, C. N. Fleming, B. D. Myron and T. J. Meyer, Rigid medium stabilization of metal-to-ligand charge transfer excited states, *J. Phys. Chem. B*, 2007, **111**(24), 6930–6941.